Electronic Supplementary Material (ESI) for Nanoscale.

Supporting Information:

Large Amplitude Charge Noise and Random Telegraph Fluctuations in Electrolyte-Gated Graphene Quantum Dots

Jasper. P. Fried[1], Xinya Bian[1], Jacob L. Swett[1], Ivan I. Kravchenko[2], G. Andrew D. Briggs[1], Jan A. Mol[1,3]

[1] *Department of Materials, University of Oxford, Oxford OX1 3PH, U.K.*

[2] *Center for Nanophase Materials Sciences, Oak Ridge National Laboratory, Oak Ridge, TN 37830, United States of America*

[3] *Department of Physics, Queen Mary University, London, E1 4NS, U.K.*

Email: jan.mol@materials.ox.ac.uk

Contents

1 Electrode Passivation

Our devices utilize a 8% PMMA495 in anisole passivation to cover the gold electrodes. This passivation layer is necessary to reduce parasitic Faradaic currents resulting from electrochemical reactions likely between ions and impurities in the gold electrodes [1]. To evaluate the effectiveness of this passivation layer we have measured the Faradaic current between a Ag/AgCl and gold electrode as a function of applied voltage for a for a non-passivated device and a device with a PMMA passivation layer. As shown in Fig. 1(a) we see a clear decrease in the measured Faradaic current when the device is passivated. Note, however, that we observe a slight Faradaic current (averages to ∼50 pA at -600 mV bias) even in the devices passivated by PMMA [inset to Fig. 1(a)]. This is potentially due to degradation of the PMMA from high electric field gradients when biasing in solution [2, 3]. Such Faradaic current can not explain the current-voltage relation observed in the main body of this work. Fig. 1(b) compares *I*-*t* traces measured on a passivated and non passivated device at zero bias. The passivation layer also significantly reduces capacitive noise resulting from coupling to the solution. The area of each gold electrode is ∼20 000 μm^2 (all of which is covered by PMMA).

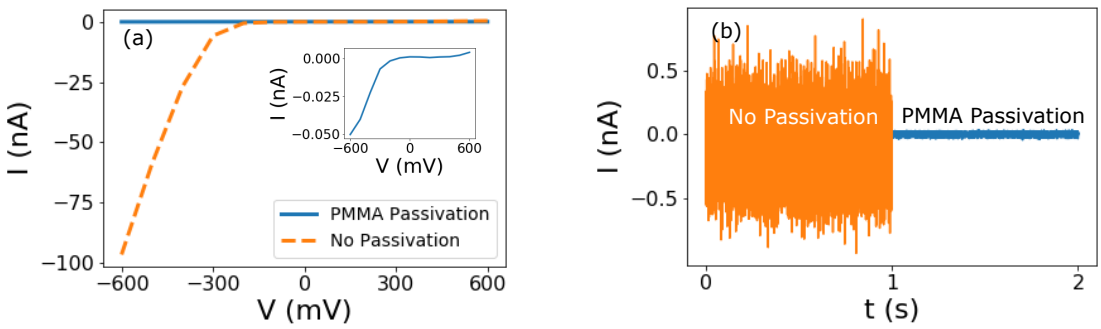

Figure 1: (a) Parasitic Faradaic current measured between a gold electrode and a Ag/AgCl electrode as a function of applied bias for a non-passivated and PMMA passivated device. The inset shows a zoom of the measured current for a PMMA passivated device. (b) *I*-*t* traces for a non passivated and PMMA passivated device measured on the gold electrode at zero bias.

2 Liquid Gated Graphene Quantum Dot Examples

Figure 2 shows three more examples of the electron transport through a graphene quantum dot controlled by an electrolyte gate.

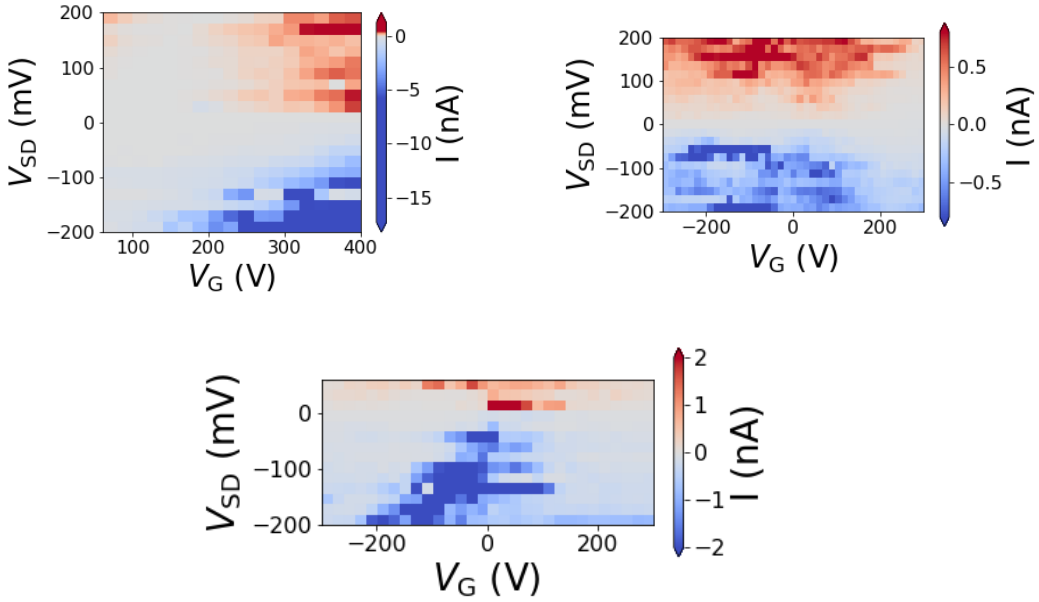

Figure 2: Examples of electron transport through a graphene quantum dot controlled by an electrolyte gate.

3 Rate Equation

The rate equation was used to obtain a fit to the measured current [4]:

$$I_{\mathrm{mar}} = \frac{e}{\hbar}\frac{\gamma_S\bar{\gamma_D} - \bar{\gamma}_S\gamma_D}{\gamma_S + \gamma_D + \bar{\gamma_S} + \bar{\gamma_D}} \tag{1}$$

where e is the electron charge, $\hbar$ is the reduced Plank's constant, $\gamma_{S/D}$ are the electron transfer rates from the source/drain electrodes to the quantum dot and $\bar{\gamma}_{S/D}$ are the electron transfer rates from the quantum dot to the source/drain electrodes.

The electron transfer rates at an electrode can be calculated by:

$$\gamma = (2 - \Omega)\int f(\epsilon)k(\epsilon)d\epsilon \tag{2a}$$

$$\bar{\gamma} = (1 + \Omega)\int \big(1 - f(\epsilon)\big)\bar{k}(\epsilon)d\epsilon \tag{2b}$$

Ω is a factor to account for the spin degeneracy of a molecular energy level and takes the value of 0 or 1 [5]. $f(\epsilon)$ is the Fermi-Dirac distribution of electrons in the electrodes which can be calculated from $f(\epsilon) = (\exp[(\epsilon - V)/k_{\mathrm{B}}T] + 1)^{-1}$ with V the voltage applied to the electrode. $k(\epsilon)$ is the rate constant for electron transfer from the electrode to the quantum dot while $\bar{k}(\epsilon)$ is the rate constant from the quantum dot to the electrode.

The rate constants are calculated by Marcus theory [6].

$$k(\epsilon) = \frac{1}{\pi}\Gamma\sqrt{\frac{\pi}{4\lambda k_B T}}\exp\left(-\frac{(\lambda + \epsilon - \mu)^2}{4\lambda k_B T}\right) \tag{3}$$

$$\bar{k}(\epsilon) = \frac{1}{\pi}\Gamma\sqrt{\frac{\pi}{4\lambda k_B T}}\exp\left(-\frac{(\lambda - \epsilon - \mu)^2}{4\lambda k_B T}\right) \tag{4}$$

Γ is the electronic coupling between the electrode and the quantum dot, λ is the reorganization energy, k_B is Boltzmann's constant, T is the temperature, ϵ is the electron energy and μ is the chemical potential of quantum dot.

The chemical potential of the quantum dot is calculated from the capacitances to the source (C_S), drain (C_D) and gate (C_G) electrodes [7].

$$\mu = c - A(C_S V_S + C_D V_D + C_G V_G) \tag{5}$$

Where the c is an offset determined by the ground state of the quantum dot and A is a constant determined by the charging energy of the quantum dot.

Fits for the experimental data shown in the main body of this work were calculated using these equations with λ, Γ_S, Γ_D, C_S, C_D, C_G,A and c the fitting parameters.

4 Field Sensitivity of GQD compared to a Graphene Ribbon

Figure 3 shows the change in current for a 20 mV change in V_G for a 500 nm wide graphene ribbon and a GQD. The GQD is approximately 10x more sensitive to change in the V_G. This partially explains the large charge noise observed in GQD devices compared to 500 nm wide graphene ribbons. Note that the exact values for the percentage change in current will depend on the applied V_G for both device geometries. This plot is simply designed to demonstrate the high sensitivity of GQD devices to changes in the electric potential.

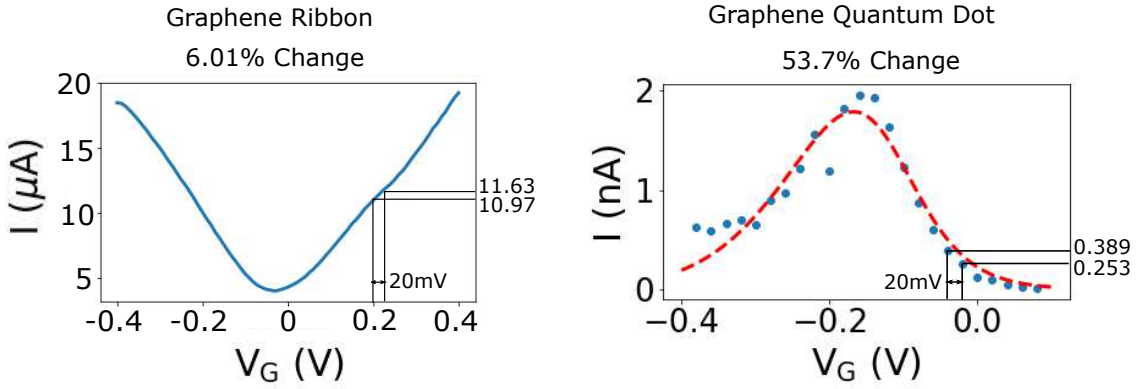

Figure 3: Change in current for a 20 mV change in V_G for a 500 nm wide graphene ribbon (left) and a graphene quantum dot (right). The dashed red line shows the fit to the experimental data.

5 Numerical calculation of Transconductance

Figure 4 plots the $|dI/dV_G|$ as calculated from a numerical derivative of the measured current as a function of V_G for V_{SD}=120 mV. This plot also shows the measured rms noise as a function of V_G for V_{SD}=120 mV. Clearly, the measured rms noise does not follow $|dI/dV_G|$ as calculated from the numerical derivative of our data. This demonstrates that our results are not introduced as a artifact of the fitting process.

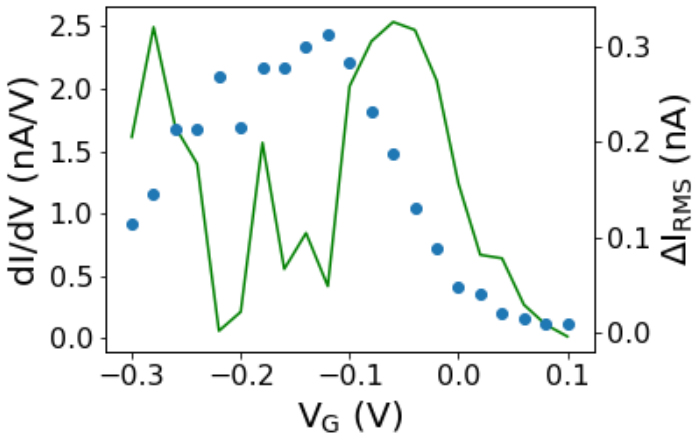

Figure 4: Transcoducate as a function of V_G for V_{SD}=120 mV as calculated from a numerical derivative to the measured data (left axis). RMS nosie as a funciton of V_G for vsd=120 mV (right axis).

6 Noise on a Different Substrate

We measured devices on a different substrate to understand the effect of the substrate on the measured noise. These devices were fabricated on top of a degenerately n-doped Si wafer with 300 nm of thermally grown SiO_2. A 3 um wide gate electrode was defined via photolithography and e-beam evaporation of 5 nm Cr followed by 30 nm of Au. A 10 nm layer of HfO_2 was then deposited via atomic layer deposition. Finally, source-drain contacts were defined either side of the gate electrode via photolithography and e-beam beam evaporation of 5 nm Cr and 50 nm Au. A graphene quantum dot was fabricated at the center of the gate electrode via the electroburning technique describe in the main body of the text.

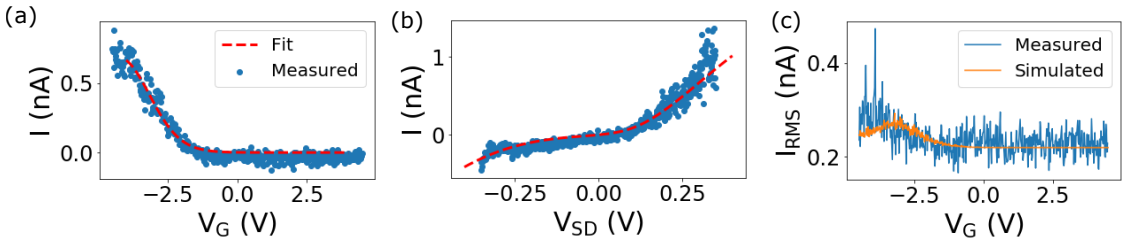

Figure 5: (a) Measured current as a function of V_G for V_{SD}=300 mV. Measured current as a function of V_{SD} for V_G=-4 V. The corresponding fits to the rate equation are shown by the red dashed lines. (c) Measured (blue) and simulated (orange) rms noise as a function of V_G for V_{SD}=300 mV.

Figure 5(a) shows the measured current as a function V_G for V_{SD}=300 mV and the corresponding fit to the rate equation. Figure 5(b) shows the measure current as a function of V_{SD} for V_G=-4 V and the corresponding fits to the rate equation. Figure 5(c) shows the measured rms noise as a function of V_G for V_{SD}=300 mV along with the rms noise of the simulated traces. In these devices the capacitive noise is much larger due to the close proximity of the Au electrode to the device. Hence a constant rms noise of 0.22 nA is added to the simulated noise level. Fluctuations in V_{SD} and V_G take the same form as that described in the body of the paper, however, here gate fluctuations were multiplied by a factor of 9.88. This factor was

calculated from the capacitances extracted from the fits to the rate equation and accounts for the different lever arm of the liquid gated and local back gated devices. The simulated and measured rms noise values match fairly well.

References

[1] K. Healy, V. Ray, L. J. Willis, N. Peterman, J. Bartel, and M. Drndić. Fabrication and characterization of nanopores with insulated transverse nanoelectrodes for DNA sensing in salt solution. *Elecrophoresis*, 33(23):3488–3496, 2012.

[2] Yuksel Temiz, Anna Ferretti, Yusuf Leblebici, and Carlotta Guiducci. A comparative study on fabrication techniques for on-chip microelectrodes. *Lab on a Chip*, 12(22):4920, 2012.

[3] Seungbeom Choi, Jeong-Wan Jo, Jaeyoung Kim, Seungho Song, Jaekyun Kim, Sung Kyu Park, and Yong-Hoon Kim. Static and dynamic water motion-induced instability in oxide thin-film transistors and its suppression by using low-k fluoropolymer passivation. *ACS Applied Materials & Interfaces*, 9(31):26161–26168, jul 2017.

[4] J. K. Sowa, J. A. Mol, G. A. D. Briggs, and E. M. Gauger. Beyond marcus theory and the landauer-bttiker approach in molecular junctions: A unified framework. *The Journal of Chemical Physics*, 149(15):154112, 2018.

[5] J. O. Thomas, B. Limburg, J. K. Sowa, K. Willick, J. Baugh, G. A. D. Briggs, E. M. Gauger, H. L. Anderson, and J. A. Mol. Understanding electron transfer on the single-molecule level. *arXiv:1812.07562*, 2018.

[6] R. A. Marcus. On the theory of oxidation-reduction reactions involving electron transfer. i. *The Journal of Chemical Physics*, 24(5):966–978, may 1956.

[7] R. Hanson, L. P. Kouwenhoven, J. R. Petta, S. Tarucha, and L. M. K. Vandersypen. Spins in few-electron quantum dots. *Reviews of Modern Physics*, 79(4):1217–1265, 2007.